Viscoelastic damping and wave cut off of titanium alloy and lattices

K. Goyal*, Z. Rueger†, E. Davis*, R. S. Lakes*+
* Department of Engineering Physics and Department of Materials Science,
University of Wisconsin, Madison, WI 53706
†Kansas City National Security Campus, Kansas City, MO 64147.
The Department of Energy's Kansas City National Security Campus is operated
and managed by Honeywell Federal Manufacturing and Technologies, LLC
under contract number DE-NA000383116.
+ Corresponding author. rlakes@wisc.edu

June 19, 2023

Abstract

3D printed titanium alloy Ti5553 solid and octet truss lattice specimens were studied via resonant ultrasound spectroscopy, free decay of vibration and quasi-static methods to determine viscoelastic damping. Damping in solid alloy and a lattice was between 10^{-4} and 10^{-3}. Much of the damping at high sonic frequency is attributed to stress induced heat flow between heterogeneities due to 3D printing. Pulsed wave ultrasound experiments disclosed reverberation in the cell structure of the lattice. Continuous wave ultrasound experiments showed that the transmissibility in the lattice rolls off beginning at about 50 kHz and becomes negligible above 110 kHz. By contrast, the polymer PMMA, though it is viscoelastic, readily transmits waves up to 1 MHz. The cut off frequency in the lattice is associated with the structure size, not intrinsic damping in the alloy. The octet truss lattice, in addition to providing good mechanical performance, is also an ultrasonic metamaterial.

1 Introduction and rationale

Viscoelastic damping of metals and lattices is of interest in the context of vibration abatement. Most structural metals have low viscoelastic damping which renders them vulnerable to vibration in applications. For example, aluminum alloys [1] and brass [2] can have viscoelastic $\tan \delta$ below 10^{-5} in the kHz frequency range. High damping metals are known: copper-manganese alloys and shape memory alloys can have high damping at high vibration amplitudes; zinc-aluminum alloys provide damping capability over a range of amplitudes; pure zinc has damping of about 10^{-2}.

Structure on the micro or milli scale can influence both static and dynamic properties. Quasi-static elastic properties of titanium alloy and lattices made from titanium alloy have been studied [4]; moduli are consistent with predictions from homogenization theory and response in the presence of spatial gradients is consistent with weak Cosserat elasticity. Rib lattice structures have long been known [3]; they are of recent interest because they can be made on a micro or milli scale via 3D printing. The octet truss lattice [3], for example, is stretch dominated and is stiffer [5] than low density foams made of the same material.

Waves in heterogeneous materials are known to be blocked at high frequency. Cut off frequencies occur at which waves are blocked in lattices of atoms [6], periodic zeolites, elastic grid lattices, corrugated fibers and dielectric materials [7], periodic particulate composites [8], materials with a periodic distribution of cavities [9] and polymer foams [10]. Resonances of rib elements in a lattice have been used to design lattices to focus sound [11].

As for the octet lattice, vibration damping has been studied recently. Hollow turbine blades with a core made of octet lattice offer improved ratios of strength to weight in comparison with solid blades [12]. Lattice filled blades were found to have have higher fundamental and third mode natural frequencies compared with solid blades made of the same Inconel 718 alloy. Damping ratios were near 0.02; solid and lattice filled blades had similar damping. Panels with octet lattices of cell width 12 cm and rib thickness 1 mm were found to ameliorate vibration via local resonance of the ribs [13].

This research deals with viscoelastic damping of titanium alloy solid specimens and octet lattices over a range of frequencies from subsonic to ultrasonic via resonant ultrasound spectroscopy, vibration free decay, and quasi-static methods. Pulsed wave and continuous wave ultrasound experiments were also conducted to explore lattice response at high frequency.
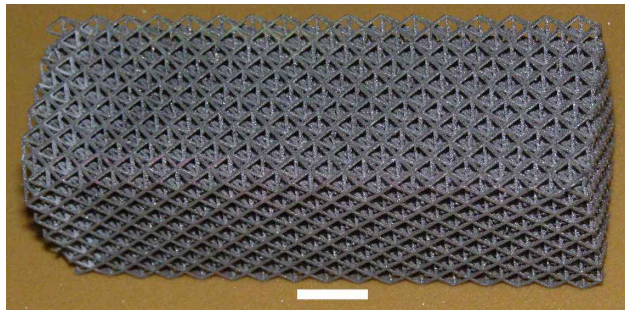
2 Methods

Figure 1: Titanium alloy octet rib lattice. Scale bar: 1 cm.

2.1 Materials

Specimens studied included solid titanium alloy rods 6.504 mm in diameter and 50 mm long as well as lattices of octet truss structure Figure 1 made of the same titanium alloy. This lattice specimen was prismatic in shape about 28 mm by 28 mm by 78 mm long and was 6 cells wide. End pieces originally provided for quasi-static elasticity studies of the lattice were sawn off to simplify interpretation of ultrasonic studies. Rib lattices had a cell size $L_c = 4.5$ mm in principal directions. The ribs visible at the surface were at an angle $45°$ with respect to principal directions and had a length $L_r = L_c/\sqrt{2}$. Rib thickness w_r was about 0.53 mm. Lattices were from two to seven cells wide in square cross section; the long direction was three times the width. The masses of specimens were determined using an analytical balance. Dimensions were measured with a micrometer. Density was calculated from mass and dimensions.

Titanium-5553 rods 2 inches long and 1/4 inch in diameter were built on a Renishaw AM250 laser powder bed fusion LPBF system using a reduced build volume in the orientation shown in Figure 2. One rod was built in the center of the build plate parallel to the plate normal z-axis, two were built perpendicular to the plate normal along the x and y axes, and 2 more were built at 45

degrees to the plate normal and 90 degrees from each other on the x-y plane. Columnar supports were used for all rods other than the central rod. These supports were selected based on prior successful builds and were slender enough to be manually broken from the rods once removed from the build plate via wire-EDM. The Renishaw AM250 is a LPBF system using single pulsed laser maximum power $P_{max} = 500$ W, wavelength $\lambda = 1070$ nm, spot size $= 70\mu$m. The titanium rods and supports were built using power ranging from 100 - 200W depending on geometry and feature. Layer thickness was 60μm. The diameter was selected because it allowed for a meandering laser scanning strategy to be used which eliminated overlapping, that may be areas of inconsistency, caused from a striped laser scanning strategy. In a meandering scanning strategy neighboring scan vectors are equally spaced and in opposite directions over the entire layer. Each layer was rotated 67 degrees to avoid stacking of scan corners and interior seams. An Additive Industries AI MetalFAB1
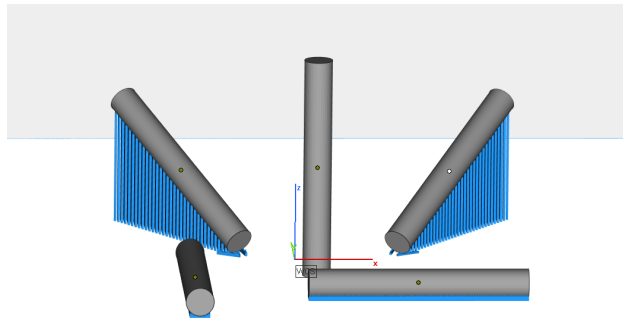

Figure 2: Design of 3D printed titanium rods.

LPBF system processing Titanium-5Al-5Mo-5V-3Cr, Ti-5553, manufactured the lattice specimens. The AI MetalFAB1 employs four full-field Ytterbium Yb doped fiber lasers $P_{max} = 500$ W, $\lambda = 1070$ nm, and spot size 100 - 105 μm to build parts with a continuous wave exposure strategy. The lattice portion and solid bases of each part were fabricated using previously developed build parameters. Laser power ranged from 120 to 160 W within both the lattice and base volumes while laser speed ranged from 600 to 950 mm/s depending on geometry. Layer thickness was constant at 40 μm. All parts were printed such that their longitudinal axes were perpendicular to the surface of the build plate. Each build layer was consolidated by the lasers using scan path striping. Scan path striping is a laser scanning strategy that divides the area to be consolidated into smaller sets of laser raster vectors. As with the solid rods, for the lattices, each layer was rotated 67 degrees to avoid stacking of scan corners and interior seams. The specimens were then removed from the build plate via wire-electrical discharge machining wire-EDM.

2.2 Resonant ultrasound spectroscopy

Resonant ultrasound spectroscopy Figure 3 reveals the mode structure and the width of the resonant peaks. The mode structure permits inference of elastic moduli and the width of the peaks allows inference of viscoelastic damping. As with all methods for materials of low damping, the inferred damping is an upper bound because there is parasitic damping. For RUS, the source is energy loss into the transducers from contact with the transducers. Resonant ultrasonic spectroscopy RUS experiments were done using Panametrics 1 MHz broadband longitudinal transducers and 1 MHz shear transducers [15], excited by a Tektronix AFG 3051c arbitrary function generator. Cylinders were supported by edges and the lattice was supported by corners to reduce parasitic damping from energy loss into the transducers. Sinusoids of different frequency was varied to

Figure 3: RUS configuration: 6 mm cylindrical specimen in edge contact with ultrasonic transducers.

explore resonances. Input and output signals were observed using a Tektronix DPO 3014 digital oscilloscope. Experiments were repeated after reorienting the specimen. There was some variation in output signal attributed to the effect of contact with the transducers.

To find the damping in the longitudinal mode of vibration, the specimen was placed between longitudinal ultrasonic transducers. For longitudinal modes, the expected fundamental natural frequency was first calculated from the density and the quasi-static value of the modulus. The longitudinal wave velocity v for waves much longer than the cylinder diameter is given by $v = \sqrt{\frac{E}{\rho}}$ and the fundamental frequency in longitudinal mode is given by $f_0 = \frac{1}{2L}\sqrt{\frac{E}{\rho}}$. Using the Young's modulus obtained from prior quasi-static studies [4] the fundamental frequency in longitudinal mode for the solid cylinder is near 42 kHz and the fundamental frequency in longitudinal mode for the lattice is near 8.4 kHz. The higher modes of longitudinal vibrations are anticipated at integral multiples of fundamental frequency i.e. f_0, $2f_0$, $3f_0$.

The method of resonant peak width was used to infer the damping $\tan\delta$ from the resonance curves. The traditional half maximum 50% maximum approach, $\tan\delta = \frac{1}{\sqrt{3}}\frac{\Delta f_{50}}{f_0}$ for those peaks that were sufficiently higher than the baseline signal. For those peaks that were split, the widths at amplitudes 80% and 90% of maximum were used rather than the traditional half maximum. For example at 80% maximum, $\tan\delta = \frac{4}{3}\frac{\Delta f_{80}}{f_0}$ with f_0 as the natural frequency and Δf as the width. This was derived using the same approach [14] as that used for the traditional half width approach.

Damping in torsion modes of vibration was determined via RUS as follows. Shear ultrasonic transducers were used to preferentially excite torsion modes. Cylinders were in contact with the transducers at their edges and prisms were in contact at their corners to minimize parasitic damping due to loss of energy to the transducers. The fundamental frequency in torsion mode for a cylinder is given by $f_0 = \frac{1}{2L}\sqrt{\frac{G}{\rho}}$; this was applied for the 3D printed titanium cylinders. When the length is equal to the specimen diameter as for the 6 mm long specimens, the lowest mode is the fundamental torsion mode, provided the material has a positive Poissons ratio and does not deviate much from isotropy. This expression is used to obtain an approximate of the fundamental torsion mode of the lattice specimen, where L is the axial length. If the material is isotropic, Poissons ratio can be inferred from the mode structure. The higher modes of torsion mode vibrations occur at integral multiples of fundamental frequency i.e. f_0, $2f_0$, $3f_0$. There was some variation in the received voltage amplitude and slight drifting of the peak. Hence, while recording the readings, it was verified that the resonance frequency and received voltage amplitude was the same before and after the width of the resonance peak was recorded.

4

During the experiments, the shear actuator and the shear sensor were placed on separate platforms to prevent the actuator vibration from affecting the sensor signal. A paper sheet was placed between the specimen and the lower transducer to eliminate electrical conduction of signal through the specimen.

These steps enabled elimination of the baseline signal to less than 1 mV compared with the recorded signals which were 100 mV to 10 V. As the contact force between the transducer and the specimen contributes to parasitic damping, the specimen was mounted with the lowest achievable contact force between the transducer and the specimen. After the test completion, the specimen was released by moving the top transducer up by a maximum of 1 micrometer division.

In shear experiments, it was difficult to identify frequencies corresponding to the higher modes of torsion. This is because frequency peaks corresponding to different and higher mode shapes lie very close to each other. Hence to identify the torsion modes in cylinder following concepts are used: (i) The frequencies of torsion modes in 50 mm long cylinders are obtained and they are approximately in the ratio 1:2:3. These frequency values are used to obtain expected frequency values of torsion modes in smaller specimens. (ii) When the edges of the cylinder align with the shear direction of the transducers, maximum shear response is obtained. When rotated by 90 degrees about the points of contact, the shear response ideally vanishes or reduces significantly.

2.3   Free decay method

Damping via free decay of vibration was determined as follows. The specimen was suspended via a string from the center, which is a vibration node for the fundamental and for higher modes. It was placed near a microphone and was tapped with a small hammer. Vibration signals were captured from the microphone on an oscilloscope. The decrease of vibration amplitude with time was analyzed to reveal the damping. Lattice specimens with solid alloy end pieces were studied via the free decay method. A lattice specimen, 32 mm by 32 mm by 96 mm long exhibited a lower natural frequency of 1.8 kHz, permitting study of lower frequency than was possible with the lattice without end pieces. As for parasitic damping, the sources of energy loss include radiation of sound and loss into the support string; the latter is minimized by using a compliant string and locating it at a vibration node where motion is minimal.

2.4   Wave ultrasound method

In addition to resonance studies, ultrasonic tests were done on the lattice so as to obtain a better understanding of the role of the lattice rib structure. One transducer was used for sending in ultrasound waves along the length of the specimens, while the other was used to detect the transmitted waves. Pulsed wave experiments were done by sending a burst of sinusoidal cycles through the lattice specimen. For comparison, similar experiments were done with a 25 mm diameter PMMA (polymethyl methacrylate) polymer rod for comparison. All pulsed tests were done at intervals of 10 ms in which the output of one pulse does not affect the output of the subsequent pulses. Bursts of sinusoidal signal 2 cycles in length at 10 ms intervals were used as input. Continuous wave ultrasonic tests were also done on the lattice by transmitting continuous sine waves of varying frequencies and determining transmissibility. Longitudinal transducers were pressed against the flat ends of the specimens with the help of a C clamp. Water was used for the PMMA specimen to enhance the coupling between the specimen ends and the transducers.

2.5 Broadband viscoelasticity BVS method

The broadband viscoelasticity spectroscopy BVS method allows viscoelastic measurements over a wide range of frequency from sub-audio to resonant studies at 100 kHz or more [16]. Such performance can be achieved for specimens that are sufficiently slender so they are structurally compliant. The instrument allows torsion or pure bending tests upon the same specimen. Torque is applied via an electric current through a Helmholtz coil. This generates a magnetic field which acts upon a high intensity magnet cemented to the specimen. Angular displacement is measured via a laser beam reflected from a mirror on the specimen upon a position sensitive silicon detector. The specimen is free at one end and fixed at the other end via a steel rod 25.4 mm in diameter. At low frequency, the resolution of phase angle is limited by the lock-in amplifier used to make the measurement.

3 Results

3.1 Moduli and damping

The density of the $45°$ solid specimen was 4.8 g/cc. The density of the $0°$ solid specimen is unknown because it was not a perfect cylinder; it had a longitudinal flat. For that reason, bounds were given for the quasi-static modulus. For resonance interpretation its density was assumed to be the same as that of the $45°$ specimen.

In RUS experiments, resonances in longitudinal vibration of solid rods were observed near 42 kHz as anticipated. A second harmonic at about twice this frequency was also observed. Each specimen was tested in a different orientation and the average longitudinal mode damping was obtained.

Moduli inferred from resonance were similar to the moduli from quasi-static measurements. Specifically, at 1 Hz, Young's modulus $E = 76$ GPa and 89 GPa for $45°$ and $90°$ rods respectively and ≥ 86, 74 GPa for $0°$ rods oriented in orthogonal directions. This last specimen was provided with a longitudinal flat; the section shape impeded calculation of the area moment of inertia. For the 42 kHz vibration frequency, Young's modulus $E = 83$ GPa and 87 GPa for $45°$ and $90°$ rods respectively; $E = 77$ GPa assuming its density to be 4.8 g/cc, the same as that of the $45°$ specimen.

As for the solid alloy shear modulus, at 1 Hz, $G = 27$ GPa and 27 GPa for $45°$ and $90°$ rods respectively and ≥ 20 GPa for $0°$ rods oriented in orthogonal directions. At 32-34 kHz, the first torsion mode of the 37 mm long specimen, the corresponding shear moduli were 28 GPa, 30 GPa, and 28.8 GPa. At 197-215 kHz, the first torsion mode of the 6 mm long specimens, the corresponding shear moduli were 27.3 GPa, 29.3 GPa, and 28.2 GPa. The differences are attributed to heterogeneity associated with 3D printing.

The first two modes of longitudinal vibration were distinctly visible. There are two possible frequencies for third mode. For the fourth mode onwards the output signal becomes too weak to be measured.

Damping via RUS in the longitudinal direction for Ti5553 37 mm long solid specimens was 5.9 $\times 10^{-3}$ for $0°$, 2.18 $\times 10^{-3}$ for $45°$ and 1.4 $\times 10^{-3}$ for $90°$. Repeated measurements after re-mounting the specimen disclosed a variance of 3% to 10%. This variance is attributed to effects of variation of contact force. However, subsequent measurements via free decay of vibration revealed that these RUS values of damping were dominated by energy loss into the transducers.

Damping in bending near 16 kHz via the method of free decay of vibration was 6.8 $\times 10^{-4}$ for $0°$, 7.8 $\times 10^{-4}$ for $45°$ and 6.1 $\times 10^{-4}$ for $90°$.

Damping of a $90°$ solid rod via BVS was 1.8 $\times 10^{-4} \pm 1.8 \times 10^{-4}$ at 1 Hz and 3.5 $\times 10^{-4} \pm 1.8$

$\times 10^{-4}$ at 10 Hz. The uncertainty in the damping arises from the phase resolution limit of the lock in amplifier. Because the specimen was relatively structurally rigid, higher frequencies were not studied because the desired mismatch of acoustic impedance with the support rod was insufficient.

Table 1: Solid Ti5553 37 mm long specimen torsion mode damping.

Specimen	f_1 kHz	$\tan\delta_S$ at f_1	f_2 kHz	$\tan\delta_S$ at f_2	f_3 kHz	$\tan\delta_S$ at f_3
0°	32	2.1×10^{-3}	63.5	9.8×10^{-4}	94.5	2.6×10^{-4}
	37	1.7×10^{-3}	64.2	6.2×10^{-4}	95	4.3×10^{-4}
45°	33	3×10^{-3}	65	3.4×10^{-4}	97	2×10^{-4}
			67	6.4×10^{-4}	98	4×10^{-4}
90°	34	4.4×10^{-3}	67.7	4.2×10^{-4}	101.3	2.4×10^{-4}
			70		102	
			70.6	6.8×10^{-4}	102.6	2.4×10^{-4}
			70.8	3.8×10^{-4}	102.7	2.2×10^{-4}

Table 2: Solid Ti5553 6 mm long specimen torsion mode damping.

Specimen	f_1 kHz	$\tan\delta_S$ at f_1	f_2 kHz	$\tan\delta_S$ at f_2	f_3 kHz	$\tan\delta_S$ at f_3
0°	197	5.1×10^{-4}	389	3.5×10^{-4}	587	2.3×10^{-4}
					590	2.2×10^{-4}
					602	1.8×10^{-4}
45°	209	4.2×10^{-4}	425	3.1×10^{-4}	615	2.2×10^{-4}
					624	2.6×10^{-4}
90°	215	4.6×10^{-4}	430	2.2×10^{-4}	646	1.8×10^{-4}

Tables 1 and 2 present torsion mode damping values of solid alloy cylinder specimens. As the resonance peaks of different mode shapes become dense at higher frequencies, it becomes difficult to uniquely identify higher torsion modes. Results for multiple modes are reported because they are meaningful even if the vibration mode is not torsional. In the 37 mm long 90 degree solid cylinder, mode splitting is observed at 70 kHz and 102 kHz. It is likely that these two correspond to second and third modes of torsion respectively as the 90 degree specimen is slightly anisotropic. The splitting of the fundamental longitudinal vibration mode was also observed in the 90 degree specimen. Lower damping in the higher modes can occur from frequency dependence of the damping. Also, parasitic damping due to energy loss from transducer contact is known to be higher in the fundamental than in the higher modes. Comparison with other results indicates the high damping observed in the fundamental mode and some of the higher modes is due to parasitic damping. The corresponding points are omitted from the summary plot.

The lattice density was found to be 0.534 g/cm^3. Because titanium has a density of 4.6 g/cc, the density divided by the density of the solid is $\frac{\rho}{\rho_s} = 0.116$. Lattice longitudinal damping results are shown in Table 3 for RUS no end pieces on specimens. Variance of 3% to about 11% in damping by the RUS method is attributed to effects of variation of contact force. The number of cells in the table refers to the width. For specimens 4, 3, and 2 cells wide, the mode with the lowest damping is shown. Further lattice longitudinal damping results are shown in Table 4 for the free decay method

specimens with end pieces and in in Table 5 for specimens without end pieces.

Table 3: Lattice $\tan \delta_L$ via RUS.

Mode	frequency kHz	$\tan \delta_L$
6 cell First f_1	8.1	8.0×10^{-4}
Second f_2	16.2	9.8×10^{-4}
Third f_3	24.4	8.1×10^{-4}
4 cell	24.6	5.4×10^{-4}
3 cell	32.7	3.7×10^{-4}
2 cell	50.9	5.6×10^{-4}
2 cell	56.8	4.5×10^{-4}

Table 4: Lattice $\tan \delta_L$ via free decay of vibration: lattices with end pieces.

widthcells	frequency kHz	$\tan \delta_L$
7	1.8	3×10^{-4}
4	2.8	3.5×10^{-4}
3	3.4	5.1×10^{-4}
2	4.8	4.8×10^{-4}

Table 5: Lattice $\tan \delta_L$ via free decay of vibration: lattices without end pieces.

width, cells	frequency kHz	$\tan \delta_L$
7	6.9	5×10^{-4}
6	8.1	5.5×10^{-4}

Table 6: Lattice torsional $\tan \delta_S$ via RUS.

Mode	frequency kHz	$\tan \delta_S$
First f_1	7.1	8.53×10^{-4}
Second f_2	14.0	5.67×10^{-4}

Table 6 presents the torsion mode damping in the lattice. The first and second torsion mode vibrations are distinctly visible. Beyond 20 kHz, where the third mode is expected, the higher modes are small in amplitude. There are many modes with similar amplitude. These modes are weaker than the first and second torsion modes, and the density of these modes is very high. At higher frequencies, beyond 150 kHz, modes are too weak to be recorded.

Figure 4 shows the free vibration response of a lattice specimen 6 cells wide. The amplitude of the free vibration decays via the equation $\ln \frac{A_2}{A_1} = -\frac{\pi tan\delta(t_2 - t_1)}{T}$ where A_1 is the amplitude at time
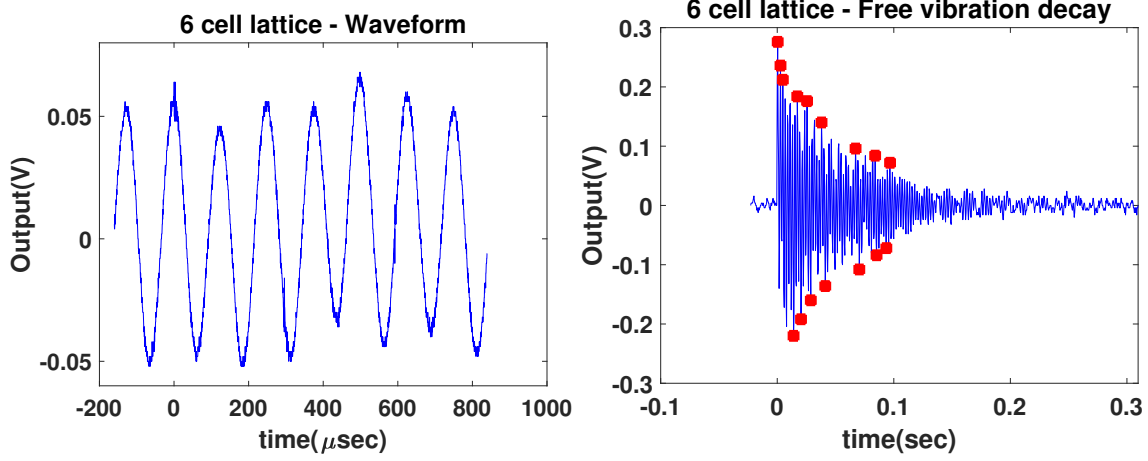
Figure 4: Free vibration decay of the lattice. Left, initial part of waveform showing the period; right, free decay of vibration. The red colored points highlight logarithmic decay of amplitude

t_1 and A_2 is amplitude at time t_2. These are local extrema of the sinusoidally varying signal. T is the time period of the vibration, while $tan\delta$ is the viscoelastic damping, which is obtained from this experiment.

The waveform period T was obtained from an expanded plot of the waveform, the graph on the left in Figure 4. The amplitude ratio was obtained from the graph on the right, from the red colored points, Ideally all the local maximum or local minimum points should follow the logarithmic decrement. The presence of multiple modes renders the waveform more complicated than an ideal waveform.The time period is approximately 124 μs which corresponds to 8.06 kHz. This is approximately the same as the fundamental frequency of the longitudinal vibration obtained from RUS. The damping is found to be 5.5×10^{-4}. This is less than the damping 8.5×10^{-4} obtained from the RUS but is similar to the damping of the second mode. The difference can be attributed to the parasitic damping due to the contact between the ultrasound transducers and the specimen. The impulse force caused slow swing of the specimen with respect to the microphone; this was too slow to obtrude in the results. Damping due to radiation of sound in longitudinal or bending modes is typically of concern if damping is less than 10^{-4}; for such materials, measurements may be conducted in an evacuated chamber.

The lattices with end pieces resonated at a lower frequency than the lattices without as a result of the additional inertia. Damping tended to increase with frequency in this regime.
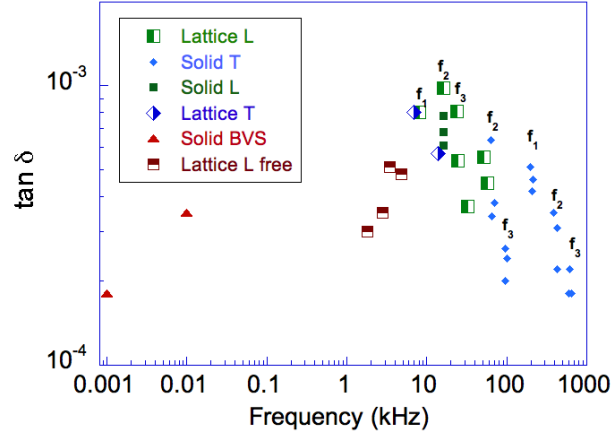
9

Figure 5: Summary of damping tanδ vs frequency. Solid points: solid specimens.

Inferred values of tan δ of solid alloy and lattices vs frequency are summarized in Figure 5. Values that were clearly raised by parasitic damping, such as nearby modes with high apparent damping, are not included in this plot.
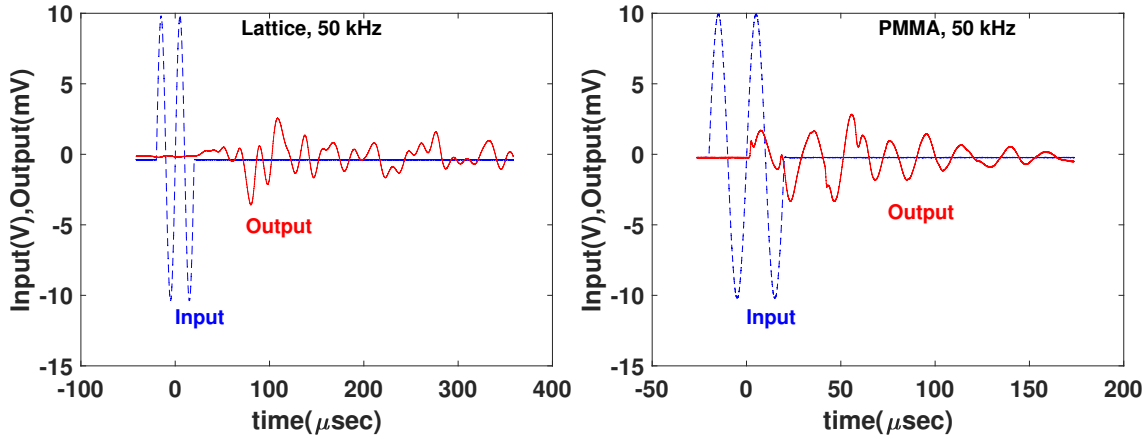
3.2 Ultrasonic wave transmission

Figure 6: Pulsed ultrasonic results for lattice left and PMMA right specimens at 50 kHz. Preamplifier gain: 10 for the lattice.

The results of pulsed ultrasonic tests at different frequencies are summarized in Figures 6 - 10.

Waveforms received in the PMMA specimen, at all the observed frequencies, resembled the input waveform. At lower frequencies the output also contained echos of diffracted input which reflect off the curved side surface. At higher frequencies, these diffracted signals are not observed. The received signal was an attenuated version of the input signal following a time delay. Signal amplitude is not a measure of attenuation because the ultrasonic transducers, with a natural frequency of 1 MHz, respond more strongly near that frequency than at lower frequencies. Indeed the transmitted signal tends to increase with frequency despite the attenuation in this viscoelastic polymer which has a tan δ of about 0.02 at ultrasonic frequency.
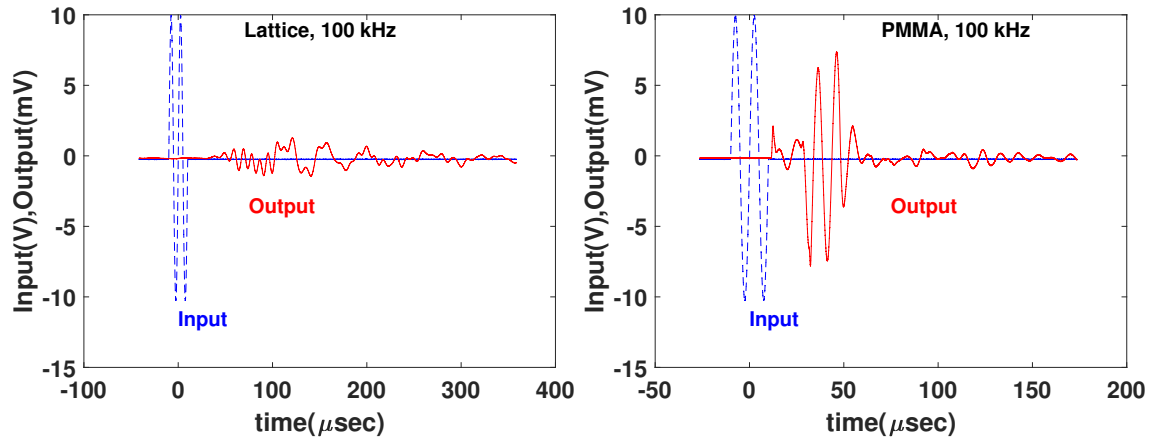
Figure 7: Pulsed ultrasonic results for lattice left and PMMA right specimens at 100 kHz. Preamplifier gain: 10 for the lattice.
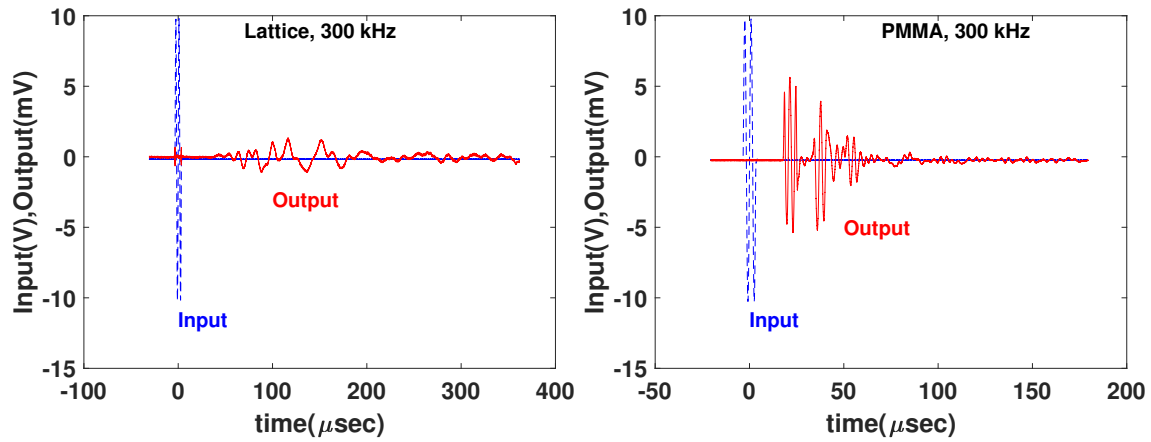

Figure 8: Pulsed ultrasonic results for lattice left and PMMA right specimens at 300 kHz. Preamplifier gain: 10 for the lattice.
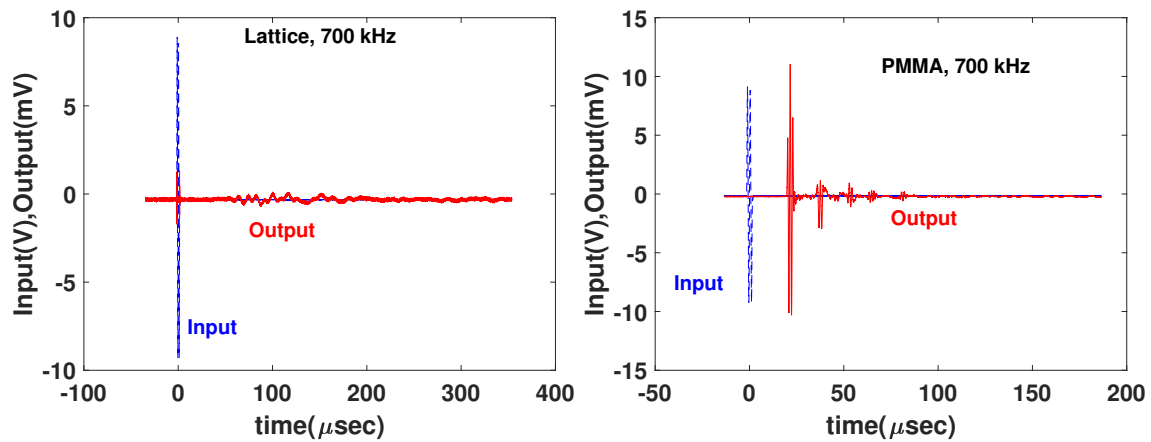

Figure 9: Pulsed ultrasonic results for lattice left and PMMA right specimens at 700 kHz. Preamplifier gain: 10 for the lattice.
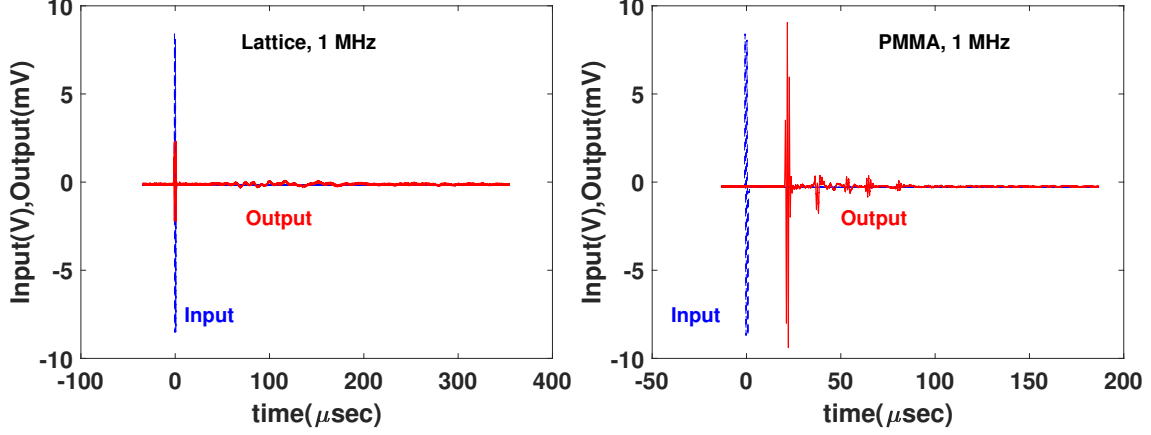
Figure 10: Pulsed ultrasonic results for lattice left and PMMA right specimens at 1000 kHz. Preamplifier gain: 10 for the lattice.
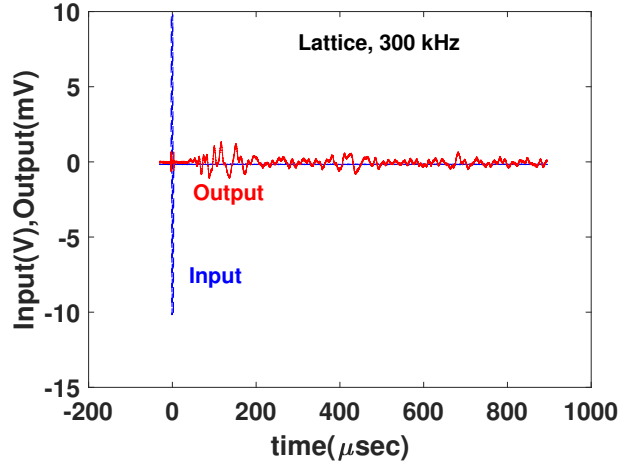

Figure 11: Pulsed ultrasonic results for lattice at 300 kHz on a longer time scale

When compared with the waveforms in PMMA, waveforms in the titanium alloy lattice at lower frequencies showed distortion of the transmitted pulse as well as reverberations over longer time scales see figure 11. At higher frequencies the signal transmitted through the lattice became progressively weaker.

The reverberations in the lattice are predominantly due to the vibration of the ribs. The fundamental natural frequency f for a simply supported bar [17] of Young's modulus E, density ρ, length L and area moment of inertia I in bending is, with q as mass per unit length, and $I = \frac{1}{12}w^4$, so $f = \frac{\pi}{2}[\frac{EI}{qL^4}]$.

For a bar of square cross section thickness w, $q = \rho w^2 L/L$, so

$$f = \frac{\pi}{4\sqrt{3}}\frac{w}{L^2}\sqrt{\frac{E}{\rho}}. \tag{1}$$

If $E = 80$ GPa, $L = 3.3$ mm, $w = 0.53$ mm, then $f = 93$ kHz.

12

For a bar free at both ends, [18] $f = 2\frac{5.6}{\pi L^2}\kappa\sqrt{\frac{E}{\rho}}$ with κ as the radius of gyration. This leads to

$$f = \frac{5.6}{\pi\sqrt{3}}\frac{w}{L^2}\sqrt{\frac{E}{\rho}}. \tag{2}$$

This frequency is higher by a factor of about 2.3 than that in Equation 1 but is of the same order of magnitude. In the lattice, the ribs are neither fully constrained nor fully free.

This analysis Equation 1 suggests that the ribs will vibrate at around 110 kHz and higher. The reverberations in the pulsed ultrasonic tests are not seen in high ranges of frequencies. Indeed, the transmissibility of the lattice figure 12 is maximum near 40 kHz, rolls off above about 50 kHz and is negligible beyond 110 kHz.
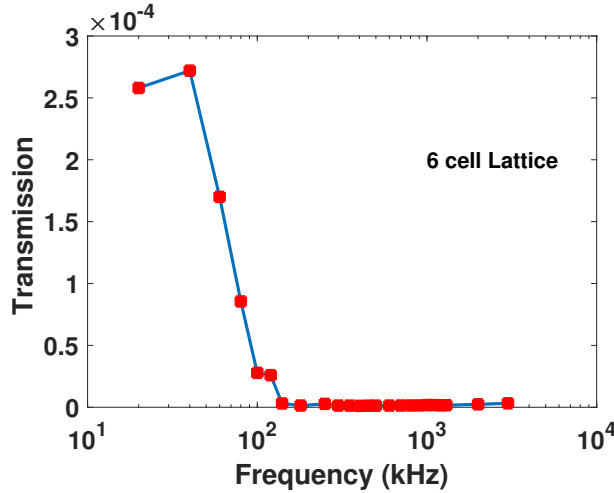

Figure 12: The ultrasonic transmissibility of the lattice vs. frequency. The experimental data points are shown in red. The blue curve shows the trend.

The observed cut off frequency may also be interpreted by comparing the cell size with the wavelength. From the prior quasi-static studies, Young's modulus E for the lattice was obtained as 0.95 GPa, hence the velocity $v = f\lambda = \sqrt{\frac{E}{\rho}} = 1334$ m/s. As the octet cell size is approximately 4.5 mm, the wavelength of input should be substantially greater than 4.5 mm for the lattice to support the waves. A wavelength of one cell size corresponds to a frequency of 296 kHz. Because each wave has two maxima and crosses zero twice, a wavelength of four cell sizes is a more appropriate measure, corresponding to a frequency of 75 kHz. The transmissibility curve figure 12 for the lattice shows that transmission rolls off above about 50 kHz and is negligible beyond 110 kHz. Similarly, the pulsed ultrasound tests on lattice show that at high frequencies the output approaches zero. In summary the lattice blocks waves above about 110 kHz in contrast to the polymer PMMA with a much higher viscoelastic tan δ which gives rise to wave attenuation.

For the lattice, tan $\delta = 5 \times 10^{-4}$ at 100 kHz corresponds to an attenuation $\alpha = 0.12$ /m or a distance of 8.5 m for waves to attenuate by a factor of $1/e$. Therefore the observed viscoelastic damping is far too low to give rise to the observed cut off of waves.

4 Causes of damping

The viscoelastic damping due to thermoelastic coupling was obtained by Zener [19]. The predicted relaxation strength is

$$\Delta = \frac{\alpha^2 T}{C_v J^S}, \tag{3}$$

with T as the absolute temperature, α as thermal expansion, J^S as the adiabatic compliance at constant entropy, and C_v as the heat capacity at constant volume. The maximum damping is half the relaxation strength

$$\tan \delta_{max} = \frac{1}{2}\Delta. \tag{4}$$

For titanium [20], $\Delta = 10^{-3}$ so the peak $\tan \delta = 5 \times 10^{-4}$. This is a substantial contribution in comparison with the damping observed. The frequency dependence for damping due to macroscopic heat flow is that of a Debye peak. The predicted frequency f_0 for peak damping from transverse thermal currents for a bar of thickness d and thermal diffusivity D, vibrating in bending [19], [21] is

$$f_0 = \frac{\pi}{2}Dd^{-2}. \tag{5}$$

For a circular rod of radius r vibrating in bending,

$$f_0 = 0.539Dr^{-2}. \tag{6}$$

Input of values for titanium [20], gives a peak at 78 Hz for a rib 1/2 mm thick, and about 0.5 Hz for a rod 6 mm in diameter. These peaks are well below the frequencies explored in the present research. The contribution of thermoelastic damping from transverse thermal currents to the total observed at ultrasonic and at high sonic frequency will be minimal.

Stress induced thermal currents between crystals or other heterogeneities also contribute to the damping [2]. The contribution of inter-crystalline thermal currents to the total damping is quantified by the quantity R which multiplies the total available relaxation strength; R has been calculated for some cubic materials. For aluminum [22], $\Delta = 0.0046$; $R = 0.0024$ and for brass, $\Delta = 0.0036$, $R = 0.18$. Titanium has hexagonal close packed symmetry. No value of R is known for titanium but titanium crystals have substantial anisotropy. Single crystal compliance elements are [24], in TPa^{-1}, $s_{11} = 9.62$, $s_{12} = -4.67$, $s_{44} = 21.5$, $s_{33} = 6.84$, $s_{12} = -1.81$. Heterogeneity in the titanium rods and lattices can be from the polycrystalline nature of the metal, from 3D printing, or both. For example, a heterogeneity of size 50μm would correspond to peak damping near 8 kHz. Damping was measured at sufficiently small amplitude that friction effects, which are nonlinear, do not contribute. Any effect of porosity on the thermo-elastic contribution to the damping can be shown to be minuscule [14]. As for heterogeneity in the nodes, inclusions in these alloys were found to be very rare. The microstructure has columnar grains. The surface has some roughness due to the 3D printing.

For comparison, damping in aluminum [23] can be from 6 to less than 3×10^{-6} at frequencies between 16 and 34 kHz, depending on grain size. The low damping was attributed to the fact aluminum has the smallest single crystal anisotropy of common metals, among them, titanium. Such anisotropy contributes to damping from stress induced thermal currents between the crystals or grains in polycrystalline materials or between layers in 3D printed materials.

Other damping mechanisms known to be active in metals [22] [18] include dislocation motion and motion of point defects.

5 Discussion

Solid Ti alloy rods had damping $\tan \delta$ between 1.8×10^{-4} and 7×10^{-4} depending on frequency. For comparison, aluminum alloys [1] and brass can have $\tan \delta$ less than 10^{-5}. Zinc has damping of about 10^{-2}; some of its alloys approach that value over ranges of frequency. For short solid specimens which have their fundamental torsion mode at higher frequency, the damping is on the order of 10^{-4} in torsion vibration modes. In long titanium alloy cylinders, the damping of the fundamental torsion mode is of the same order of magnitude as the damping in the longitudinal vibration mode. The damping decreases to the order of 10^{-4} in higher torsion modes. Part of that effect is attributed to the known greater effect of parasitic damping on the lower modes.

In the lattice, the damping $\tan \delta$ is between 10^{-4} and 10^{-3} for both torsion and longitudinal modes of vibration. The higher modes of the two vibration types in the lattice progressively become weaker as frequency increases.

For both solid rods and lattices, much of the damping at high sonic frequencies can result from stress induced heat flow between heterogeneities associated with the 3D printing process.

Materials prepared by 3D printing are known to exhibit deviations from the ideal design geometry and input material properties. Such deviations and uncertainties could be analyzed by numerical methods [25].

Pulsed wave ultrasound tests reveal reverberations in the lattice structure. The transmissibility of the lattice rolls off beginning at about 50 kHz and becomes negligible above 110 kHz. By contrast, the glassy polymer PMMA, though it is viscoelastic, readily transmits waves up to 1 MHz. The cut off frequency observed in the lattice is not due to intrinsic damping in the alloy comprising it because solid alloy specimens exhibited small damping on the order of 10^{-4} at frequencies in the vicinity of the cut off. The observed viscoelastic damping is far too low to give rise to the observed cut off of waves in the lattice. The physical cause of the cut off frequency is resonance of the cell ribs. The cut off frequency observed can also be viewed in the context of a generalized continuum theory with more freedom than Cosserat elasticity used to understand the quasi-static response [4] of lattices. This is the Mindlin microstructure theory [26], also called micromorphic elasticity, which allows the local rotation and strain to differ from the macroscopic rotation and strain. The octet truss lattice, intended for superior mechanical performance, is also an ultrasonic metamaterial.

6 Acknowledgment

References

[1] W. Duffy, Acoustic quality factor of aluminum alloys from 50 mK to 300 K, J. Appl. Phys. 68, 5601-5609, **1990**.

[2] R. H. Randall, F. C. Rose, and C. Zener, Intercrystalline thermal currents as a source of internal friction, Phys. Rev. 53, 343-348, **1939**.

[3] Buckminster Fuller, Octahedral building truss, US Patent 3,354,591, **1967**.

[4] K. Goyal Z. Rueger, E. Davis and R. S. Lakes, Cosserat elasticity of octet truss titanium alloy lattices, Journal of Mechanics of Materials and Structures, accepted, **2021**

[5] V. Deshpande, N. Fleck and M. F. Ashby, Effective properties of the octet truss lattice material, Journal of the Mechanics and Physics of Solids 49, 1747-1769, **2001**.

[6] L. Brillouin, Wave Propagation in Periodic Structures, Dover, New York **1953**.

[7] C. Elachi, Waves in active and passive periodic structures: a review. Proc. IEEE 64,1666-1698 **1976**.

[8] V. K. Kinra, E. Ker, An experimental investigation of pass bands and stop bands in two periodic particulate composites, International Journal of Solids and Structures 19, 393-410, **1983**.

[9] J. D. Achenbach and M. Kitahara, Harmonic waves in a solid with a periodic distribution of spherical cavities, J. Acoust. Soc. Am. 81, 595 **1987**.

[10] C. P. Chen and R. S. Lakes, Dynamic wave dispersion and loss properties of conventional and negative Poissons ratio polymeric cellular materials, Cellular Polymers, 8, 343-359 **1989**.

[11] A. C. Hladky-Hennion, J. O. Vasseur, G. Haw, C. Croenne, L. Haumesser, and A. N. Norris, Negative refraction of acoustic waves using a foam-like metallic structure, Appl. Phys. Lett. 102, 144103 **2013**.

[12] S. Hussain, W. A. W. Ghopa, S. S. K. Singh, A. H. Azman, S. Abdullah, Experimental and numerical vibration analysis of octet-truss lattice based gas turbine blades, Metals, 12, 340 **2022**. https://doi.org/10.3390/met 12020340

[13] G. Aguzzi, A. Colombi, E. N. Chatzi, Vibration mitigation via octet lattice structures, 3rd International Conference on Natural Hazards and Infrastructure Athens, Greece, 22-24 June, **2021**. https://doi.org/10.3929/ethz-b-000520521

[14] R. S. Lakes, *Viscoelastic materials*, Cambridge University Press, Cambridge **2009**.

[15] Y. C. Wang and R. S. Lakes., Resonant ultrasound spectroscopy in shear mode, Review of Scientific Instruments, 74, 1371-1373, **2003**.

[16] T. Lee, Lakes, R. S. Lakes, and A. Lal, Resonant ultrasound spectroscopy for measurement of mechanical damping: comparison with broadband viscoelastic spectroscopy, Review of Scientific Instruments, 71 2855-2861, July **2000**.

[17] H. Benaroya, *Mechanical vibrations*, Prentice Hall, New Jersey **1998**.

[18] A. S. Nowick and B. S. Berry, *Anelastic Relaxation in Crystalline Solids*, Academic, New York, **1972**.

[19] C. Zener, Internal friction in solids I - Theory of internal friction in reeds, Phys. Rev. 52, 230-235, **1937**.

[20] K. B. Milligan and V. K. Kinra, On the thermoelastic damping of a one-dimensional inclusion in a uniaxial bar, Mechanics Research Communications, 20, 137-142, **1993**.

[21] C. Zener, Internal friction in solids II. General theory of thermoelastic internal friction, Phys. Rev. 53, 90-99, **1938**.

[22] C. Zener, *Elasticity and anelasticity of metals*, University of Chicago Press, Chicago, **1948**.

[23] C. Zener, Internal friction of aluminum, Phys. Rev. 58, 472-473, **1940**.

[24] R. F. Hearmon, The elastic constants of crystals and other anisotropic materials. In: Hellwege K. H., Hellwege A. M., Eds., *Landolt-Bornstein Tables*, Group III, Vol. 11, Springer-Verlag, Berlin, pp 1-154 **1979**.

[25] P. Hauseux J. S. Hale, S. P. A. Bordas, Accelerating Monte Carlo estimation with derivatives of high-level finite element models, Computer Methods Appl. Mech. and Eng., 318, 917-936, **2017**.

[26] R. D. Mindlin, Micro-structure in linear elasticity, Arch. Rational Mech. Analy, 16, 51-78, **1964**.